J. Phys. B: At. Mol. Opt. Phys. **44** (2011) 235002 (6pp) doi:10.1088/0953-4075/44/23/235002

Non-isotropic angular distribution of Yb Lα_1 and Lα_2 lines following photoionization by linearly polarized radiation

Cahit Karanfil[1] **and Raul A Barrea**[2]

[1] Department of Physics, Faculty of Science, Muğla University, 48187 Muğla, Turkey
[2] BioCAT, Biophysics Collaborative Access Team, Illinois Institute of Technology, IL 60616, USA

E-mail: rbarrea@gmail.com

Received 25 August 2011, in final form 18 October 2011
Published 11 November 2011
Online at stacks.iop.org/JPhysB/44/235002

Abstract
The angular distribution of Yb Lα_1 and Lα_2 lines after photoionization by a linearly polarized monochromatic photon beam from synchrotron radiation has been measured. The experiment was performed using a 5×5 μm^2 x-ray beam and a high-resolution detection system designed for this experiment to resolve the Lα_1 and Lα_2 emission lines. The main advantage of the proposed experimental configuration is the elimination of geometrical effects, ensuring the independence of the experimental results from previously seen geometrical pitfalls. The experimental value of the degree of alignment parameter A_{20} shows very good agreement with the predicted theoretical value.

(Some figures in this article are in colour only in the electronic version)

1. Introduction

The decay of the L_3 subshell vacancies following an ion–atom collision and electron–atom collision has been investigated experimentally [1–12] and theoretically [13–17] for many decades. It is well established that vacancies created in such ion–atom collisions with angular momentum $J > 1/2$ are aligned. As a consequence of this alignment, the angular distributions of the Auger electrons and the characteristic x-rays are non-isotropic and the characteristic photons are polarized. In the case of photoionization, Flugge *et al* [18], and later McGuire [19], and Oh and Pratt [20] showed that if the total angular momentum of the ion created after the photoionization process is $J > 1/2$, then the ion will be aligned with the direction of the incident beam (because the different magnetic substates are unequally occupied). According to these conditions, excitation of the subshell $2p_{3/2}$ and higher shells with $J > 1/2$ will generate the aligned vacancies. The ion alignment will be manifested in the non-isotropic angular distribution of the Auger electrons and the non-isotropic angular distribution and polarization of the characteristic x-rays. The theoretical approaches usually limit their studies to a few groups of ions that have their subshells full or closed, ensuring that the total angular momentum of the atom is $J = 0$ and the total angular momentum of the ion is the same of the vacancy created $Jc = J$.

The experimental approaches, on the other hand, are not limited by these assumptions but instead by the availability of appropriate excitation sources and detection systems. Several groups have studied these phenomena using radioactive sources as the excitation beam, which are limited in energy tunability and photon flux delivered. The results reported are controversial, showing a wide range of values from very strong anisotropy [21–27] to a complete absence of that effect [28–30]. Synchrotron radiation was later used to determine the angular distribution of L lines of different elements taking advantage of this highly tunable and intense source of x-rays by two different groups [8, 9]. Their results also showed discrepancies; one group observed no anisotropy [9] while the other found experimental evidence of non-isotropic distribution in very good agreement with theoretical calculations [8]. The detection system, a key component of the experimental setup, did not resolve the most interesting emission lines Lα_1 and Lα_2 in both cases. These

Table 1. Anisotropy parameter α_2 of the Yb L_3 transitions (j and j' are the angular momenta of the initial and final states) taken from [32].

Line	j	j'	α_2
Lα_1	3/2	5/2	0.112
Lα_2	3/2	3/2	−0.393

lines are expected to experience opposite angular distributions due to their anisotropy coefficient α_2 (see table 1). More recently, Yamaoka *et al* [10, 31] used a flat Si crystal analyser and a position sensitive detection system to resolve the L emission lines of Au. Their results showed a non-isotropic emission after photoionization with an experimental alignment parameter larger than the theoretical calculations [10] and slightly independent of the Coster–Kronig transitions [31].

The existing experimental results are still scarce and controversial. Since the anisotropy parameters are expected to be very small, it is highly recommended to choose the best experimental conditions to reduce potential pitfalls and improve the data quality. The purpose of this paper is to report experimental results of the angular distribution of Yb Lα_1 and Lα_2 emission lines excited using linearly polarized x-ray microbeam and a high-resolution detection system. The measurements were carried out at the Biophysics Collaborative Access Team (BioCAT) beamline at the Advanced Photon Source (APS), Argonne National Laboratory (ANL). The results obtained show that the angular distribution of Yb Lα_1 and Lα_2 fluorescence lines is non-isotropic. These results are in very good agreement with the prediction of Flugge [18], Scofield [32, 33], Kleinman [34] and Berezhko [35].

2. Theory

Considering linearly polarized incident radiation with the incoming photon oriented along the z-axis, the x-ray angular distribution in the dipole approximation can be written as [36]

$$W_{\text{theoretical}}(\theta,\phi) = \frac{W_0}{4\cdot\pi}\left(1+\alpha_2\left[A_{20}\cdot P_2(\cos(\theta)) + \frac{1}{\sqrt{6}}\text{Re}\, A_{22}\cdot P_2^2(\cos(\theta))\cdot\cos(2\phi)\right]\right), \quad (1)$$

where

- W_0 is the total x-ray emission rate;
- θ is the angle measured between the characteristic x-ray and the incoming photon;
- ϕ is the azimuthal angle measured from the x direction;
- α_2 is the anisotropy coefficient for a particular transition;
- A_{20} and A_{22} the alignment parameters and
- $P_2(\cos(\theta))$ and ${P_2}^2(\cos(\theta))$ are the Legendre polynomials and associated Legendre polynomials, respectively.

In the dipole approximation, the parameters A_{20} and A_{22} are related by the following expression [34]:

$$A_{22} = A_{20}\cdot\sqrt{\tfrac{3}{2}}\cdot(-\eta_3 + \mathrm{i}\eta_1), \quad (2)$$

where η_3 and η_1 are two of the Stokes parameters.

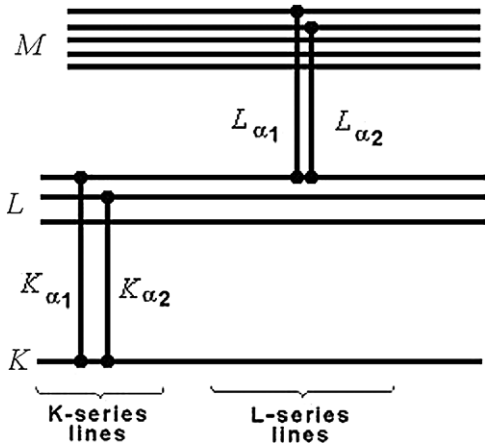

Figure 1. Energy diagram showing the K and L transitions.

For a totally linearly polarized photon beam oscillating along the x-axis, i.e. in the reaction plane x–z where $\eta_3 = 1$, $\eta_1 = 0$ and $\phi = 0$, inserting expression (2) into (1) simplifies the angular distribution to

$$W_{\text{Theoretical}}(\theta) = \frac{W_0}{4\cdot\pi}\cdot(1+\alpha_2\cdot A_{20}\cdot[\cos^2(\theta) - 2\sin^2(\theta)]). \quad (3)$$

The experimental x-ray fluorescence intensity of Yb L lines (Lα_1 or Lα_2, see the transition diagram in figure 1) emitted at angles θ when the incident energy E_0 is above the L_3 absorption edge and below the L_2 edge is described as

$$I_\chi(\theta) = \frac{\sigma_{\text{L3}}(E_0)\cdot\omega_3\cdot F_{\text{i}\chi}}{4\pi}\cdot W_\chi(\theta)\cdot I_0\cdot G(\theta)\cdot\varepsilon(E_\chi)\cdot T(E_0,E_\chi), \quad (4)$$

where

- $\sigma_{\text{L3}}(E_0)$ represents the L_3 subshell photoionization cross section;
- ω_3 is the fluorescence yield in the L_3 subshell;
- $F_{\text{i}\chi}$ is the L_3 emission rate for the χ line (Lα_1 or Lα_2) [37];
- $W_{L\iota}(\theta)$ is the experimental angular distribution of the emission lines Lα_1 or Lα_2;
- I_0 is the incident beam intensity;
- $G(\theta)$ is a geometrical factor;
- $\varepsilon(E_{Li})$ is the detector's efficiency at the emission energy $E_{\text{L}\alpha 1}$ or $E_{\text{L}\alpha 2}$, and
- $T(E_0,E_{Li})$ is the self-absorption factor that accounts for the incident and emission lines.

The requirement for the incident energy to be below the L_2 absorption edge is essential to avoid intra-shell Coster–Kronig contributions, even if these contributions have been observed to be small [31].

The ratio of the intensities $I_{L\alpha 1}(\theta)$ and $I_{L\alpha 2}(\theta)$ is expressed as

$$\frac{I_{\text{L}\alpha_1}(\theta)}{I_{\text{L}\alpha_2}(\theta)} = \frac{F_{\text{L}\alpha_1}\cdot W_{\text{L}\alpha_1}(\theta)}{F_{\text{L}\alpha_2}\cdot W_{\text{L}\alpha_2}(\theta)}. \quad (5)$$

The detector efficiency and the self-absorption factors are considered the same for each emission line, because of

the small energy difference between them ($\Delta E = 48$ eV); therefore, they cancel out in expression (5). The other atomic and geometrical factors are independent of the emission line; thus, they cancel in equation (5) as well. The $F_{L\alpha_1}/F_{L\alpha_2}$ factor is a constant value independent of the angle of emission. Theoretical values of these parameters can be obtained from Scofield [37].

Combining the experimental intensity ratio (5) with the theoretical expression (3), we obtain

$$\frac{I_{L\alpha_1}(\theta)}{I_{L\alpha_2}(\theta)} = \frac{F_{L\alpha_1}}{F_{L\alpha_2}} \cdot \frac{(1 + \alpha_{2L\alpha_1} \cdot A_{20} \cdot [\cos^2(\theta) - 2\sin^2(\theta)])}{(1 + \alpha_{2L\alpha_2} \cdot A_{20} \cdot [\cos^2(\theta) - 2\sin^2(\theta)])}. \tag{6}$$

This simple expression shows that the ratio of the experimental intensities of these two emission lines can be used to derive the alignment parameter A_{20} without the need of a secondary normalization standard, typically a Kα line from a transition metal. The calculated values for the anisotropy coefficient α_2 for Yb Lα_1 and Lα_2 lines [32] are shown in table 1.

3. Experimental details

In order to carry out the proposed determinations, the 18ID BioCAT Undulator beamline at the APS, ANL, was used [38]. The experimental set-up comprises the APS storage ring that operates at 3.7 GeV and a nominal current of 100 mA; an undulator type 'A'; a silicon (1 1 1) double crystal monochromator and a pair of Kirkpatrick–Baez (KB) focusing mirrors that provided 10^{12} Ph s^{-1} flux and a beam size of 5×5 μm^2. The use of a microbeam is required for the optimum operation and performance of a high-resolution Bent Crystal Laue Analyser (BCLA) [39, 40] because its energy resolution is a direct function of the incident beam size. The BCLA offers many advantages over a Si flat crystal analyser: it is easier to setup and to align requiring only two linear stages; the angular acceptance of the BCLA is in the order of milliradians while for the flat crystal configuration this value is in the order of microradians (very narrow reflectivity width). The analyser used in this experiment was designed to resolve the Yb Lα_1 and Lα_2 lines. An ionization chamber that measures the incident 9.2 keV beam intensity (selected to excite only the Yb L_3 edge) and a silicon drift detector used to collect the diffracted photons from the BCLA completed the experimental setup. The whole setup is mounted on a motorized lift table, which allows the vertical positioning of the instrument within the linearly polarized x-ray beam plane. A schematic of the experimental setup is shown in figure 2. A layout of the beamline and microprobe setup can be found elsewhere [41, 42].

A specially designed detector–sample holder assembly consisted of a Huber rotary stage, a sample holder and a BCLA holder arm. The rotary stage was used for the rotation of the detection system around the focal point of the microbeam. The BCLA used for this experiment consisted of an aluminium bender and a bent silicon crystal 15 μm thick with [1 0 0] surface orientation and ⟨1 1 1⟩ reflection plane. Its calculated reflectivity and asymmetry angle were 35% and 35.26°, respectively. The energy resolution of the analyser

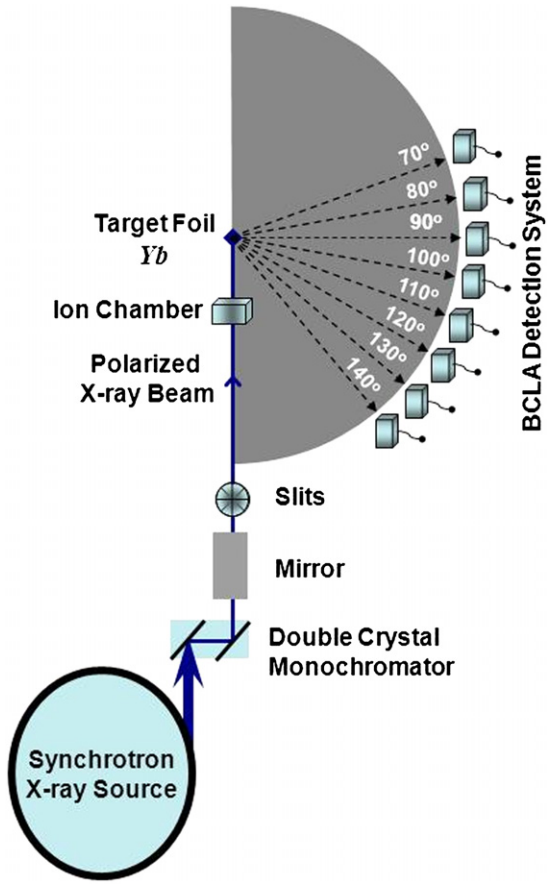

Figure 2. Schematics of the setup used. The KB mirrors system, the sample positioning and the detector holder can be seen.

is 15 eV at the Yb Lα energy lines. The BCLA alignment is performed by scanning two independent motorized linear stages. Details about how to align and operate a BCLA analyser can be found elsewhere [39]. The sample holder consisted of an aluminium support that can be easily aligned at the focal point of the microbeam. It can be mounted at different orientation angles allowing the incident beam–sample angle to be selected accordingly with the proposed experiment. A fix incident angle value of 25° was used to minimize self-absorption effects.

Thick foils, 5×5 mm^2 area, of high purity (99.9%) Yb and Ni were used as samples. Although the current measurements required no standard for normalization purposes, we have measured the distribution of the Ni Kα line to verify the stability and reproducibility of the experimental setup. We have found no deviations or distortions of the isotropic Kα lines distribution. Such thick samples provided high-intensity fluorescence emission that reduced the acquisition time during the experiment. Although the current measurements required no standard for normalization purposes, we have measured the angular distribution of Ni Kα_1 and Kα_2 lines (see the transition diagram in figure 1) to verify the stability and reproducibility of the experimental setup. For these lines, expression (6) can be simply expressed as

$$\frac{I_{K\alpha_1}(\theta)}{I_{K\alpha_2}(\theta)} = \frac{F_{K\alpha_1}}{F_{K\alpha_2}} = \text{constant}. \tag{7}$$

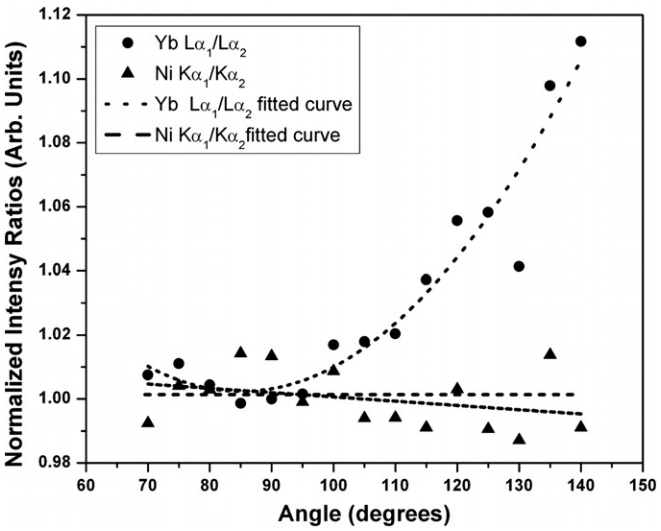

Figure 3. Experimental Ni $K\alpha_1/K\alpha_2$ and Yb $L\alpha_1/L\alpha_2$ normalized intensities ratio and curve fitting using a linear fit for Ni lines and equations (6) for Yb lines. A constant line of normalized ratio equal to 1 is also shown for comparison purposes. Note that the deviation of the Ni values from the constant value is less than 2%.

We have found no deviations or distortions of the isotropic $K\alpha$ lines distribution. A normalized intensity ratio $Ni_{K\alpha 1}/Ni_{K\alpha 2}$ is presented in figure 3.

The θ angle scans (70° to 140°, 5° steps) were performed in the x–z plane. The scanning angles were measured relative to the direction of the incident beam (see figure 2). Four independent scans were performed to determine potential instability issues. This approach allowed us to compare different scans and to further check both beamline and setup stability. No evidence of drift or shifts was found between the different scans. The final spectra were obtained from the sum of those four scans for each angle. The total acquisition time per θ angle was set to 120 s. This strategy minimized the counting statistic error: less than 1% for the $L\alpha_2$ line and less than 0.3% for the $L\alpha_1$ line.

4. Results and discussion

Yb L spectral lines measured using a BCLA detection system (energy resolution 15 eV @ Yb $L\alpha$ lines) and a silicon drift detector (energy resolution 165 eV @ Mn $K\alpha$ line) are shown for comparison purposes (figure 4). The use of a logarithmic spiral shape crystal analyser provided three orders of magnitude larger angular acceptance compared to a perfect flat crystal configuration, allowing us to collect sufficient photons in reasonable time. The BCLA improves the signal to noise (S/N) ratio by a factor of 22 compared to solid state Ge or Si detectors [40]. The combined BCLA–silicon drift detector improves this factor to about 50 times because it rejects the transmitted beam through the thin crystal by using a single channel analyser window centred on the Yb $L\alpha$ line [39]. This performance is reflected in the measured peak intensities shown in figure 5 where the experimental Yb $L\alpha_1$ and $L\alpha_2$ lines measured at 9.2 keV and $\theta = 90°$, fitted peaks and their corresponding residuals are shown. The lines were fitted using

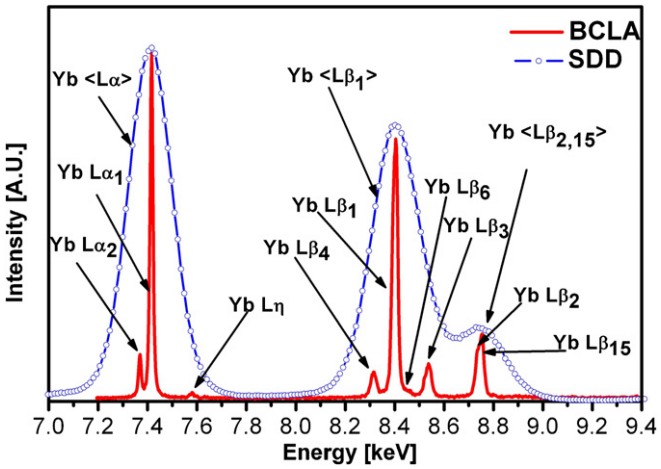

Figure 4. Yb L lines spectrum taken using the BCLA system compared to a typical Si drift detector spectrum. Note that the energy resolution of the BCLA allowed us to resolve the $L\alpha_1$ and $L\alpha_2$ lines.

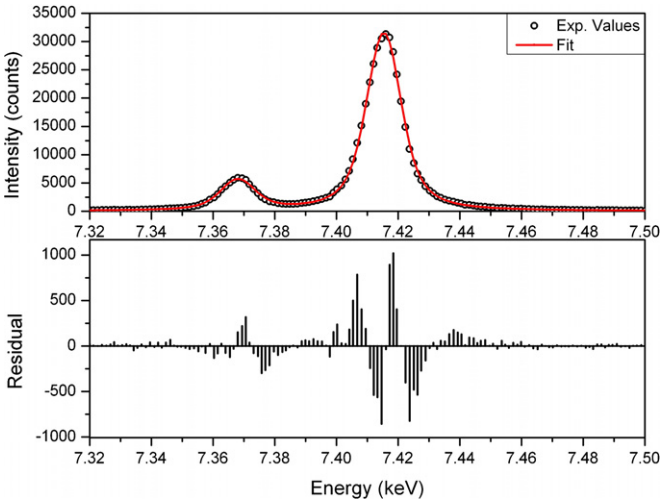

Figure 5. Yb $L\alpha_1$ and $L\alpha_2$ experimental intensities, the fitting peaks and their corresponding residuals determined at 9.2 keV excitation energy, $\theta = 90°$ and $\phi = 0°$.

a Voigt shape function. It is clearly observed in figure 5 that there is a very good fit between the measured peaks and the two Voigt fitting curves. The fitting error was determined from the square root of the sum of the residuals, between the experimental and fitted curve, squared. The total error in each spectrum was about 2%.

A nonlinear system of equations with two fitting parameters, 'C' (a normalization constant that represents the ratio $F_{L\alpha 1}/F_{L\alpha 2}$) and '$A_{20}$' (degree of alignment), was set using equation (6) for each θ angle using the experimental intensity ratios on the left-hand side of the equation and the anisotropy parameter from table 1 on the right-hand side. The estimated errors for these parameters were obtained considering the mean deviation of the measured data from the fitted curve and the uncertainties of each measured point [43].

Experimental data and fitted angular distributions of $L\alpha_1/L\alpha_2$ line ratio are shown in figure 6. The curve is a direct evidence of the non-isotropic distribution of these lines.

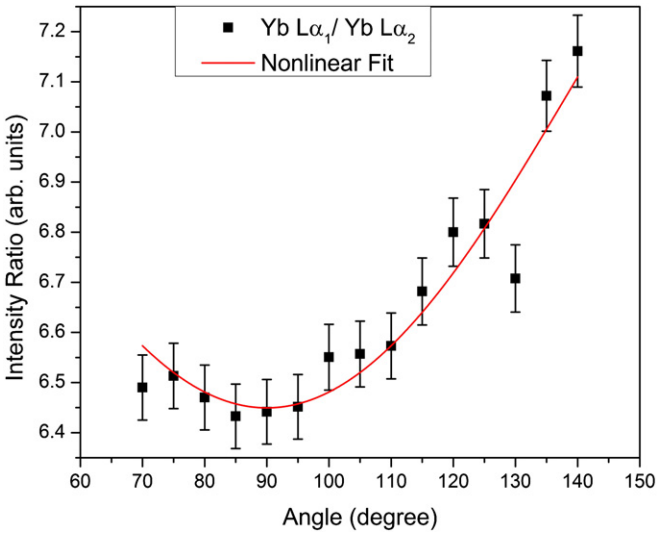

Figure 6. Experimental Yb $L\alpha_1/L\alpha_2$ intensity ratio and curve fitting using the model from equation (6).

As indicated before, by measuring the intensity ratio of these lines the experimental data are independent of the geometrical factors. Because these lines experience opposite anisotropy effects due to the α_2 parameter values (see table 1), the ratio maximizes the non-isotropic effect. The experimental value found for A_{20} is 0.113 ± 0.010.

Berezhko *et al* [35] have calculated the degree of alignment, A_{20}, for a variety of atoms and transitions. The degree of alignment has limiting values depending on the orbital and total angular momenta of the ion vacancy. In the case of the initial ion state $2p_{3/2}$, the theoretical limits are $0.1 \leqslant A_{20} \leqslant 0.35$, the smallest value corresponding to high-energy incident photon and the larger value corresponding to low energy incident photon. Our incident beam was set to 9.2 keV, which corresponds to 18.8 rydbergs above the Yb L_3 edge; therefore, the expected A_{20} value is in the low limit. The experimental degree of alignment found in the present experiments, $A_{20} = 0.113 \pm 0.010$, is about 10% higher than the tabulated value [35], which could be considered in very good agreement with the theoretical calculations.

While some potential explanations for the many discrepancies of the experimental results were presented elsewhere [8], the incident beam size and the divergence of the fluorescence photons were not considered among them. In a typical experimental configuration where the excitation beam size and the detector aperture size are in the range of millimetres, the divergence of the fluorescence x-rays could be considered a source of systematic errors. In the present experimental configuration, these pitfalls were solved by using a microbeam as a photon source and a BCLA as a detection system. The incident beam of 25 μm^2 illuminated the sample; thus, the fluorescence emission could be considered as generated from a point source and this is reflected in the energy resolution of the BCLA observed (see figure 5). This combination ensured a minimum angular divergence of the fluorescence photons. Other advantages of the detection system configuration are as follows: it is simple to setup and operate and it provides a high-background rejection compared to other detection systems [39]. The evaluation of the experimental intensities ratio of Yb $L\alpha_1$ and $L\alpha_2$ eliminated the need of secondary standards, since the geometrical effects are the same for both lines. The fitting procedure was simplified by the fact that the shape of the BCLA peaks can be represented by two Voigt shape curves, eliminating the need for complex functions [26]. The extremely low background shown in figure 5 is achieved by the use of a silicon drift detector attached to the BCLA [39].

5. Conclusions

The angular distribution of the Yb $L\alpha_1$ and $L\alpha_2$ fluorescence lines has been measured and a non-isotropic angular distribution of the $L\alpha_1$, $L\alpha_2$ lines reflected on their alignment parameter A_{20} was found; therefore, the Yb ion is aligned with the incident beam. The experimental value of this parameter ($A_{20} = 0.113 \pm 0.010$) is in good agreement with the theoretical predictions of Flugge [18], Scofield [32, 33], Kleinman [34] and Berezhko [35].

We have developed an experimental apparatus to measure the angular distribution of the fluorescence emission of Yb L lines at different angles using a linearly polarized incident microbeam and a high-resolution detection system. The use of a microbeam as the excitation source allowed us to avoid critical experimental pitfalls previously observed related to incident beam size and fluorescence divergence. The detection system provided the energy resolution and background rejection to obtain high-quality data and to avoid complex fitting procedures. The performance of currently described apparatus is very promising for further experiments and developments of this field.

Acknowledgments

BioCAT is a NIH-supported Research Center, RR08630. The use of the Advanced Photon Source was supported by the US Department of Energy, Basic Energy Science, Office of Energy Research, under contract no W-31-109-Eng-38. This research is also supported by the Turkish Council of Higher Education.

References

[1] Jamison K A and Richard P 1977 *Phys. Rev. Lett.* **38** 484
[2] Peterson E H *et al* 1975 *Phys. Rev.* A **11** 1267
[3] Scholer A and Bell F 1978 *Z. Phys.* A **286** 163
[4] Jitschin W, Kleinpoppen H, Hippler R and Lutz H O 1979 *J. Phys. B: At. Mol. Phys.* **12** 4077
[5] Kamiya M *et al* 1979 *Phys. Rev.* A **20** 1820
[6] Hitachi A *et al* 1991 *J. Phys. B: At. Mol. Opt. Phys.* **24** 3009
[7] Papp T, Campbell J L and Maxwell J A 1993 *Phys. Rev.* A **48** 3062
[8] Barrea R A *et al* 2005 *J. Phys. B: At. Mol. Opt. Phys.* **38** 839–52
[9] Yamaoka H *et al* 2002 *Phys. Rev.* A **65** 062713
[10] Yamaoka H *et al* 2003 *J. Phys. B: At. Mol. Opt. Phys.* **36** 3889–97
[11] Sharma A and Mittal R 2010 *Nucl. Instrum. Methods* A **619** 55–8
[12] Namito Y, Ban S and Hirayama H 2008 *Phys. Rev.* A **78** 033419

[13] Berezhko E G and Kabachnik N M 1977 *J. Phys. B: At. Mol. Phys.* **10** 2467
[14] Berezhko E G, Kabachnik N M and Sizov V V 1978 *J. Phys. B: At. Mol. Phys.* **11** 1819
[15] Rosel F, Trautmann D and Bauer G 1982 *Z. Phys.* A **304** 75
[16] Mehlhorn W 1994 *Nucl. Instrum. Methods Phys. Res.* B **87** 227
[17] Lohmann B and Kleiman U 2006 *J. Phys. B: At. Mol. Opt. Phys.* **39** 271–81
[18] Flugge S, Mehlhorn W and Schmidt V 1972 *Phys. Rev. Lett.* **29** 7
[19] McGuire E J 1970 Sandia Laboratories *Report No Sc-RR-70-721*
[20] Oh S D and Pratt R H 1974 *Phys. Rev.* A **10** 1198
[21] Kahlon K S *et al* 1990 *J. Phys. B: At. Mol. Opt. Phys.* **23** 2733
[22] Kahlon K S *et al* 1991 *Phys. Rev.* A **44** 4379
[23] Sharma J K and Allawadhi K L 1999 *J. Phys. B: At. Mol. Opt. Phys.* **32** 2343
[24] Ertugrul M *et al* 1995 *Nuovo Cimento* D **17** 993
[25] Ertugrul M 1996 *Nucl. Instrum. Methods Phys. Res.* B **119** 345
[26] Ertugrul M and Erdogan H 1997 *Appl. Spectrosc. Rev.* **32** 159
[27] Seven S and Kocak K 2001 *J. Phys. B: At. Mol. Opt. Phys.* **34** 2021
[28] Kumar A *et al* 1999 *J. Phys. B: At. Mol. Opt. Phys.* **32** 3701
[29] Kumar A *et al* 2001 *J. Phys. B: At. Mol. Opt. Phys.* **34** 613
[30] Mehta D *et al* 1999 *Phys. Rev.* A **59** 2723
[31] Yamaoka H *et al* 2006 *J. Phys. B: At. Mol. Opt. Phys.* **39** 2747–56
[32] Scofield J H 1976 *Phys. Rev.* A **14** 1418
[33] Scofield J H 1989 *Phys. Rev.* A **40** 3054
[34] Kleiman U, Lohmann B and Blum K 1999 *J. Phys. B: At. Mol. Opt. Phys.* **32** 309–26
[35] Berezhko E G, Kabachnik N M and Rostovsky V S 1978 *J. Phys. B: At. Mol. Phys.* **11** 1749–58
[36] Kabachnick N M and Sazhina I P 1996 *J. Phys. B: At. Mol. Opt. Phys.* **29** L515–9
[37] Scofield J H 1974 *At. Data Nucl. Data Tables* **14** 121
[38] Fischetti R *et al* 2004 *J. Synchrotron Radiat.* **11** 399–405
[39] Kujala N G, Karanfil C and Barrea R A 2011 *Rev. Sci. Instrum.* **82** 063106
[40] Karanfil C 2003 *PhD Thesis* Illinois Institute of Technology
[41] Barrea R A *et al* 2010 *J. Synchrotron Radiat.* **17** 522
[42] Barrea R A *et al* 2005 *Proc. 8th Int. Conf on X-Ray Microscopy (IPAP Conf. Series 7)* pp 230–2
[43] Rogers D W O 1975 *Nucl. Instrum. Methods* **127** 253